SUPPLEMENTARY INFORMATION, Felis

Table S1 (Supplementary Table 1) Accelerator mass spectrometry (AMS) ^{14}C dating of modern coral cores from the northernmost Red Sea.

Site	Latitude Longitude	Sample material	Lab.- ID	Calendar age (yrs AD)	[14]C age (yrs BP)	Reservoir age (yrs)	ΔR (yrs)
Ras Umm Sidd	27° 50.9' N 34° 18.6' E	RUS-95/a (*Porites* sp.)	KIA11296	1750	815 ± 25	657	273
Ras Umm Sidd	27° 50.9' N 34° 18.6' E	RUS-95/b (*Porites* sp.)	KIA11297	1750	715 ± 25	557	173
Ras Umm Sidd	27° 50.9' N 34° 18.6' E	RUS-95/1804 (*Porites* sp.)	KIA14536	1804	700 ± 30	542	166
Ras Umm Sidd	27° 50.9' N 34° 18.6' E	RUS-95/1900 (*Porites* sp.)	KIA14539	1900	590 ± 30	490	135
Aqaba	29° 27.6' N 34° 58.4' E	AQ18-1804 (*Porites lutea*)	KIA14540	1804	760 ± 35	602	226
Aqaba	29° 27.6' N 34° 58.4' E	AQ18-1900 (*Porites lutea*)	KIA14537	1900	575 ± 30	475	120

AMS ^{14}C dating was performed at the Leibniz-Labor for Radiometric Dating and Isotope Research[1] (Kiel, Germany). Sample material is from cores of two annually banded corals, core RUS-95 from Ras Umm Sidd[2] and core AQ18 from Aqaba[3]. Reservoir age and ΔR value (difference between the regional and global marine ^{14}C age) were calculated following refs. 4,5 and the Marine Reservoir Correction Database. The ΔR value of 154 years used in this study is the average of the six values determined here and five additional values taken from the Marine Reservoir Correction Database (http://radiocarbon.pa.qub.ac.uk/marine/).

SUPPLEMENTARY INFORMATION, Felis

Table S2 (Supplementary Table 2) Mean seasonal cycle of sea surface temperature in the northernmost Red Sea based on coral Sr/Ca and $\delta^{18}O$. The standard error of each mean (±1SE) and the number of years used to calculate the mean (N) are also given.

Proxy	Modern coral 1 (EILAT-15B)	Modern coral 2 (AQ2)	Modern coral 3 (EILAT-1)	Average modern corals 1-3	Modern coral 4 (Ras Umm Sidd)	Late Holocene coral (AQB-10-B)	Last interglacial coral (AQB-3-A)
Sr/Ca	5.6 °C ± 0.6	4.5 °C ± 0.3	5.2 °C ± 0.5	5.2 °C ± 0.3		5.2 °C ± 0.3	8.4 °C ± 0.4
$\delta^{18}O$	5.2 °C ± 0.2	5.3 °C ± 0.1	4.7 °C ± 0.4	5.1 °C ± 0.2	5.0 °C ± 0.1	5.2 °C ± 0.3	8.4 °C ± 0.5
	N = 7	N = 5	N = 5	N = 17	N = 244	N = 14	N = 12

SUPPLEMENTARY INFORMATION, Felis

Table S3 (Supplementary Table 3) Mean annual growth rate of the corals used in this study.

	Modern coral (EILAT-15B)	Modern coral (AQ2)	Modern coral (EILAT-1)	Late Holocene coral (AQB-10-B)	Last interglacial coral (AQB-3-A)
Growth rate (cm/yr)	1.34	1.50	0.64	0.61	1.48

SUPPLEMENTARY INFORMATION, Felis
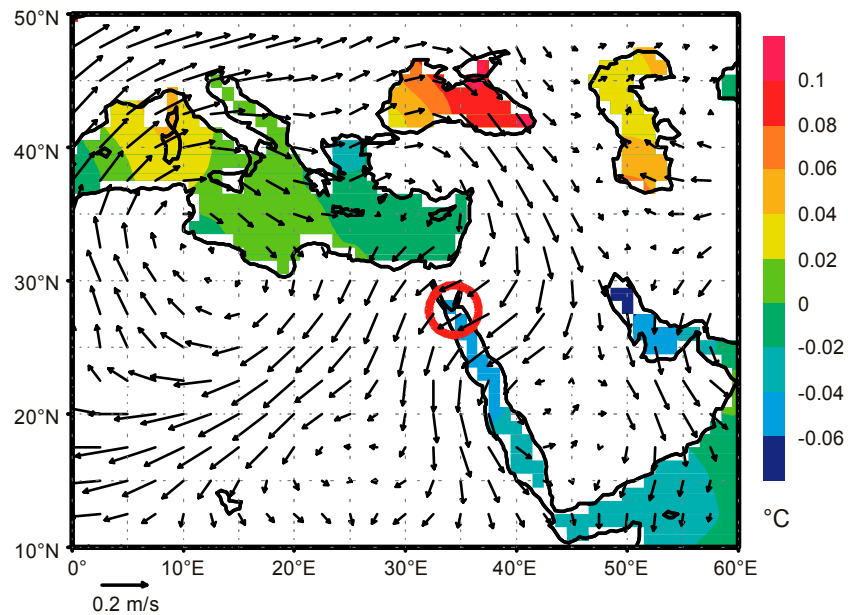
Figure S1 (Supplementary Figure 1) Relationship between a modern coral
$\delta^{18}O$ time series from the northernmost Red Sea (Ras Umm Sidd)[2] and the
regional signature of the Arctic Oscillation in the Middle East[6] for interannual
variability throughout the year. Regression of the 850 hPa wind field[7] and the
sea surface temperature field[8] against the coral $\delta^{18}O$ time series (1950-1994),
performed for bimonthly, detrended, and normalized time series with the
average seasonal cycle removed. All data were filtered in the 5-6 year band
prior to analyses. The coral location is marked by a red circle.

SUPPLEMENTARY INFORMATION, Felis
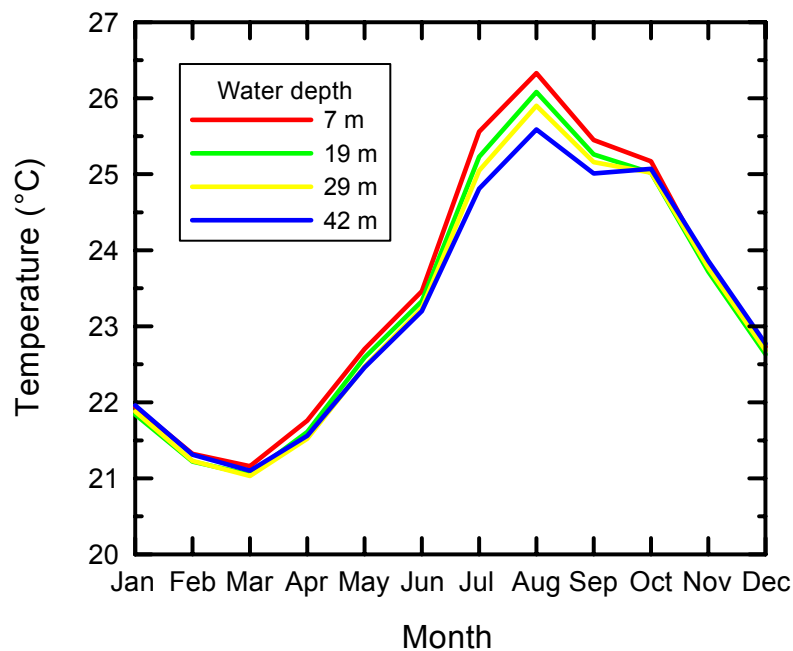
Figure S2 (Supplementary Figure 2) Mean monthly water temperature in the
northernmost Red Sea over the depth range of *Porites* coral growth. The
seasonal cycle of temperature decreases with water depth by about 0.7 °C
between 7 and 42 m depth. This results from a weak stratification of the water
column during summer. During winter the water column is well mixed. Our
modern reference corals are from shallow waters (4 to 18 m). Consequently, the
increased temperature seasonality documented by the last interglacial coral can
not be explained by a relative difference in paleo-depth. Data are based on
hourly measurements of four temperature loggers which were deployed along
the reef slope at Aqaba for the period May 1999 to November 2001.

SUPPLEMENTARY INFORMATION, Felis
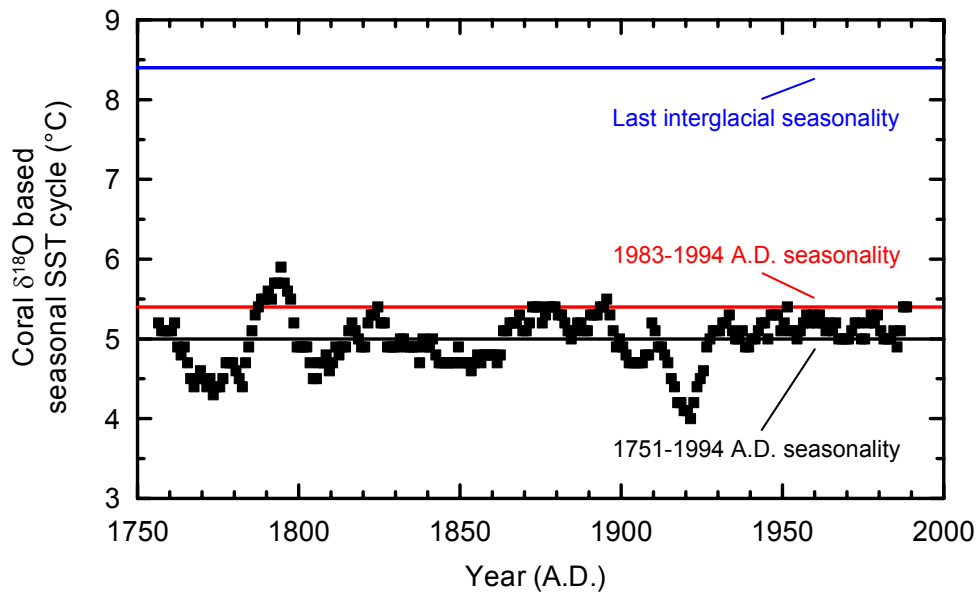
Figure S3 (Supplementary Figure 3) Coral $\delta^{18}O$ based seasonal cycle of sea surface temperature (SST) in the northernmost Red Sea during the past centuries, compared with that of the last interglacial. The mean values of a 12 year moving window are shown (squares), based on the application of our coral $\delta^{18}O$-SST relationship (see Methods) to a modern coral record from Ras Umm Sidd[2]. Horizontal lines indicate means for the period 1751-1994 A.D. (black), the most recent 12 year window (red), and the 12 year window provided by the last interglacial coral (blue), respectively. There is no 12 year window during the past approximately 250 years during which the coral based seasonal SST cycle was as high as indicated by the last interglacial coral.

SUPPLEMENTARY INFORMATION, Felis
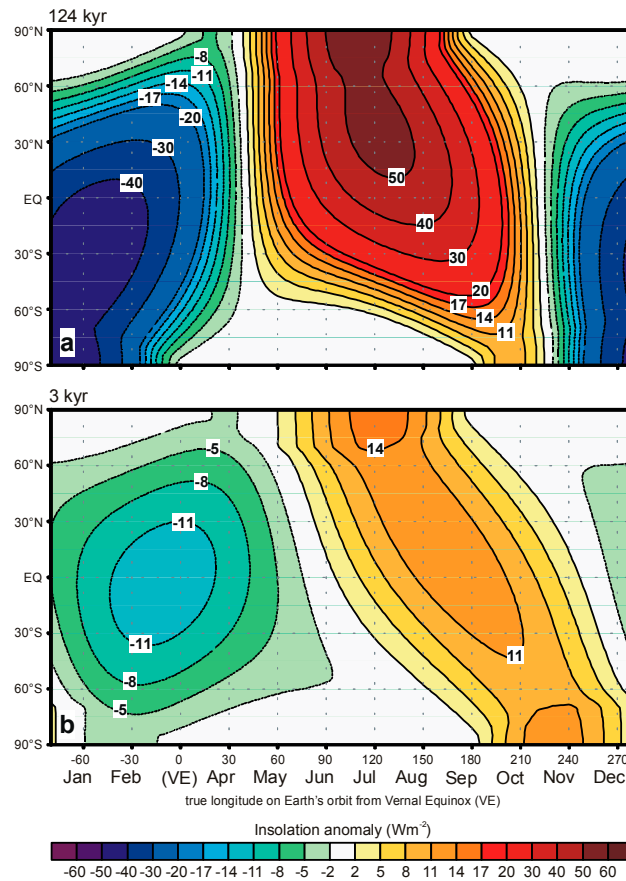
Figure S4 (Supplementary Figure 4) Insolation anomalies for the last interglacial and the late Holocene. Annual distribution of insolation anomaly relative to modern conditions for **a**, 124 kyr ago and **b**, 3 kyr ago, calculated after ref. 9. Shown is the latitudinal distribution with respect to the true longitude (angle between perihelion and vernal equinox on the Earth's orbit). Note that following Kepler's Law the track speed on the elliptical orbit varies.

SUPPLEMENTARY INFORMATION, Felis
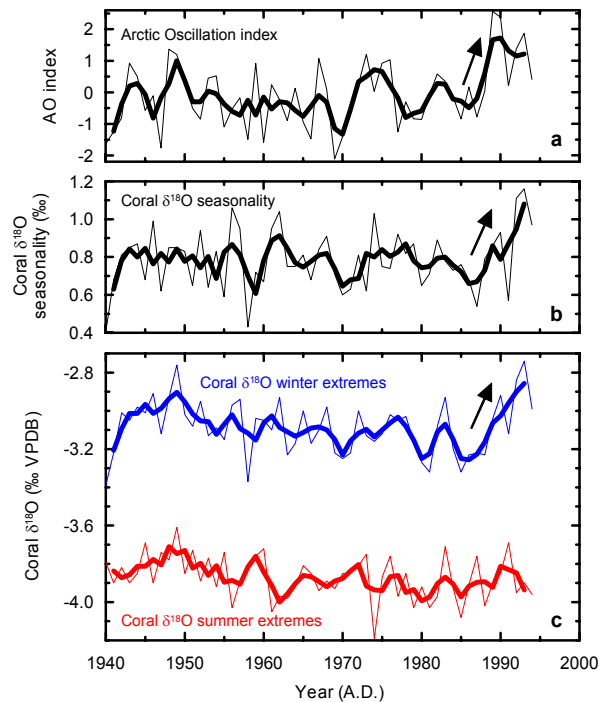
Figure S5 (Supplementary Figure 5) The Arctic Oscillation (AO) index[10] (January-March) and coral $\delta^{18}O$ seasonality in the northernmost Red Sea over the past decades. **a**,**b** A shift toward the AO high index state from the mid-1980s to the early 1990s is accompanied by increased $\delta^{18}O$ seasonality in a coral record from Ras Umm Sidd[2]. **c**, The latter results from a shift in the winter coral $\delta^{18}O$ extremes toward colder/more arid conditions whereas the corresponding summer extremes remain relatively constant. This shows that a shift toward the AO/NAO high index state is accompanied by colder winters in the northernmost Red Sea, thereby increasing the seasonal cycle of temperature in this region. Correlations of the AO index (1940-1994 A.D.) with coral $\delta^{18}O$ seasonality (r = 0.47) and coral $\delta^{18}O$ winter extremes (r = 0.54) respectively are highly significant (99.9% level, 2-sided t-test). Bold lines represent 3 year running averages.

SUPPLEMENTARY INFORMATION, Felis
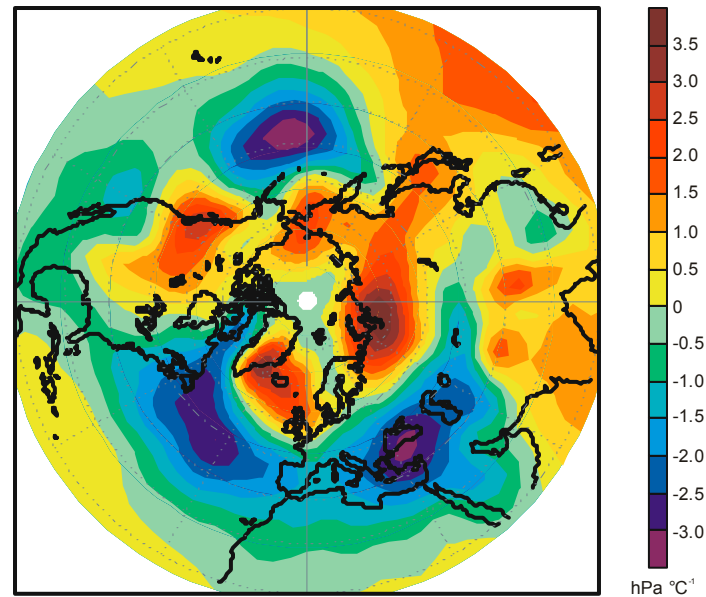
Figure S6 (Supplementary Figure 6) Relationship between the modelled sea surface temperature (SST) index of the coral region and the modelled sea level pressure (SLP) field of the Northern Hemisphere, based on the coupled atmosphere-ocean general circulation model ECHO-G. Regression of the modelled SST index covering the eastern Mediterranean and the Red Sea (see Supplementary Fig. S7 for definition) against the modelled Northern Hemisphere SLP field for the period 1820-1920 A.D. (December, January, February). Prior to the calculation the trends have been eliminated.

SUPPLEMENTARY INFORMATION, Felis
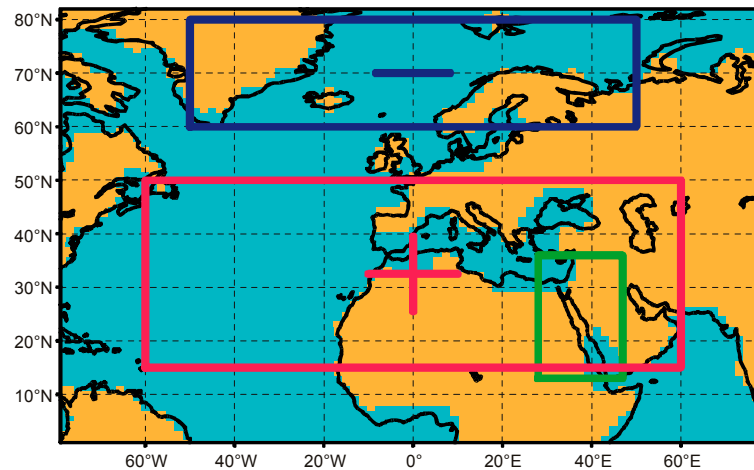
Figure S7 (Supplementary Figure 7) Definition of modelled indices used in this study. The sea surface temperature (SST) index of the coral region (Fig. 3c, e) has been obtained from the averaged modelled SST over the eastern Mediterranean and the Red Sea (28°-47° E; 13°-36° N; green box). The modelled AO/NAO index (Fig. 3f) is calculated from the sea level pressure (SLP) difference between a southerly high pressure region (60° W-60° E; 15°-50° N; red box with plus sign) and a northerly low pressure region (50° W-50° E; 60°-80° N, blue box with minus sign). The brown rectangles mark the sea-land-mask of the atmospheric submodel ECHAM4 in its T30 resolution.

SUPPLEMENTARY INFORMATION, Felis
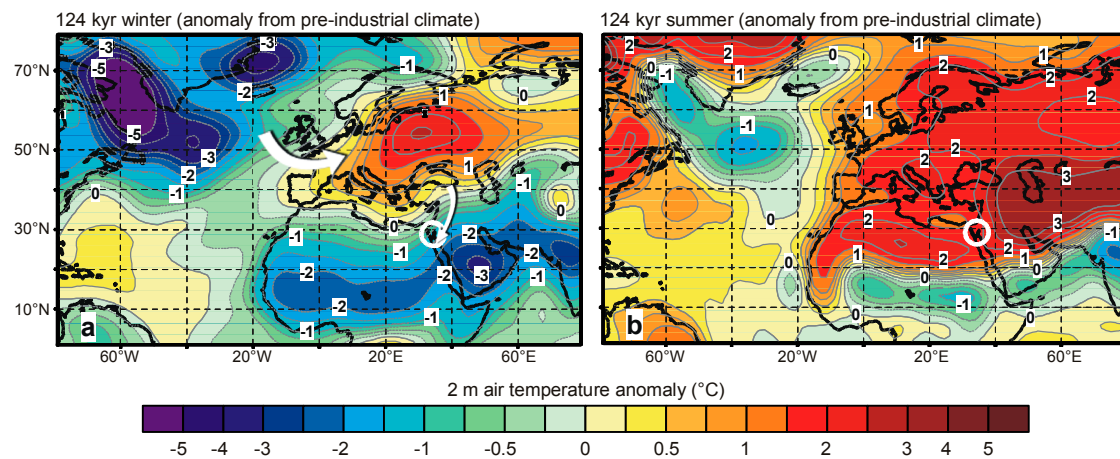
Figure S8 (Supplementary Figure 8) Near surface air temperature anomaly for the last interglacial based on the coupled atmosphere-ocean general circulation model ECHO-G. Difference between last interglacial (124 kyr) and pre-industrial climate (1820-1850 A.D.) for **a**, winter (December, January, February) and **b**, summer (June, July, August). The corresponding anomalies from modern climate are shown in Fig. 4a, b. Near surface wind anomaly is schematically represented as white arrows. An average of 11 simulation years has been applied to the last interglacial climate centred at 124 kyr. The region of coral collection in the northernmost Red Sea is marked by a white circle.

SUPPLEMENTARY INFORMATION, Felis
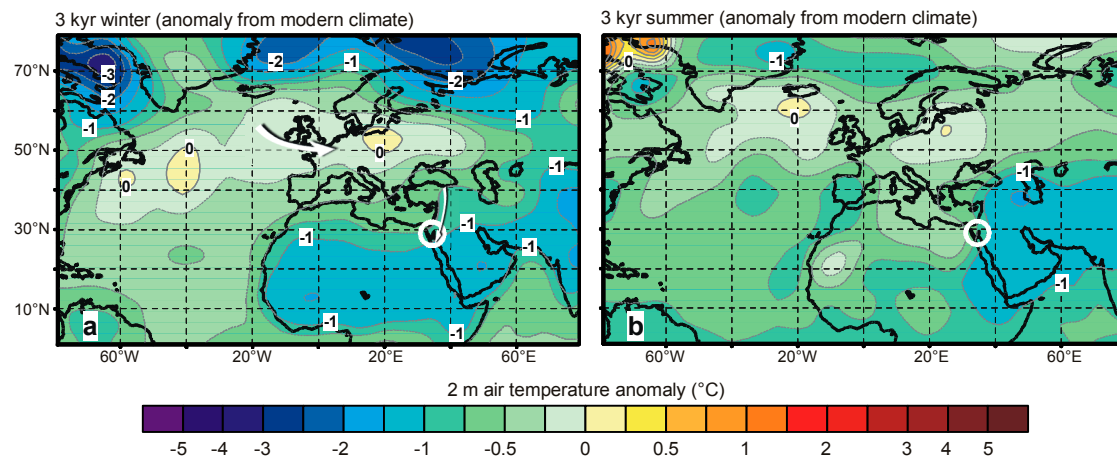
Figure S9 (Supplementary Figure 9) Near surface air temperature anomaly for the late Holocene based on the coupled atmosphere-ocean general circulation model ECHO-G. Difference between late Holocene (3 kyr) and modern climate (1975-1985 A.D.) for **a**, winter (December, January, February) and **b**, summer (June, July, August). The corresponding anomalies from pre-industrial climate are shown in Fig. 4c, d. Near surface wind anomaly is schematically represented as white arrows. An average of 11 simulation years has been applied to the late Holocene climate centred at 3 kyr. The region of coral collection in the northernmost Red Sea is marked by a white circle.

SUPPLEMENTARY INFORMATION, Felis
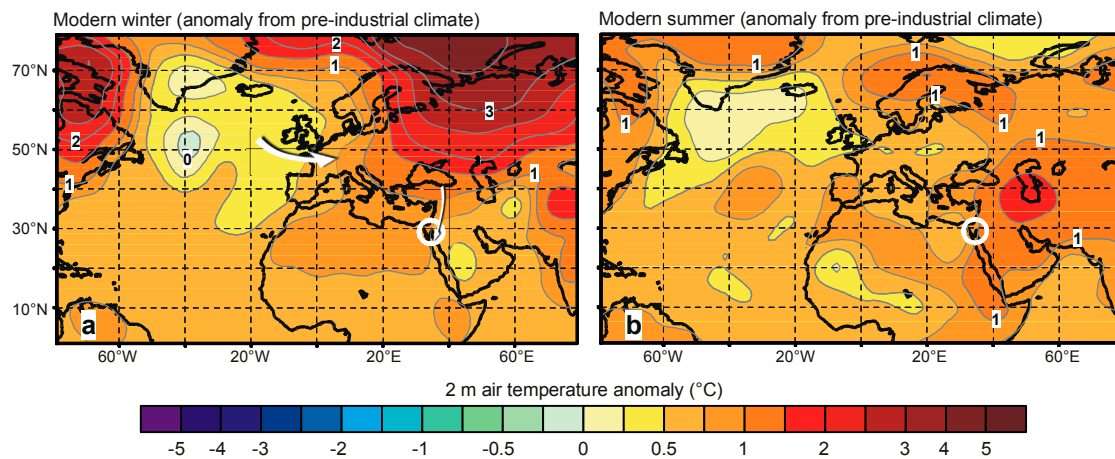
Figure S10 (Supplementary Figure 10) Near surface air temperature anomaly for modern climate based on the coupled atmosphere-ocean general circulation model ECHO-G, showing the anomalous temperature induced by the perturbation of anthropogenic greenhouse gases. Difference between modern (1975-1985 A.D.) and pre-industrial climate (1820-1850 A.D.) for **a**, winter (December, January, February) and **b**, summer (June, July, August). Near surface wind anomaly is schematically represented as white arrows. The greenhouse gas concentrations are based on ice core and instrumental records[11-14]. The region of coral collection in the northernmost Red Sea is marked by a white circle.

SUPPLEMENTARY INFORMATION, Felis
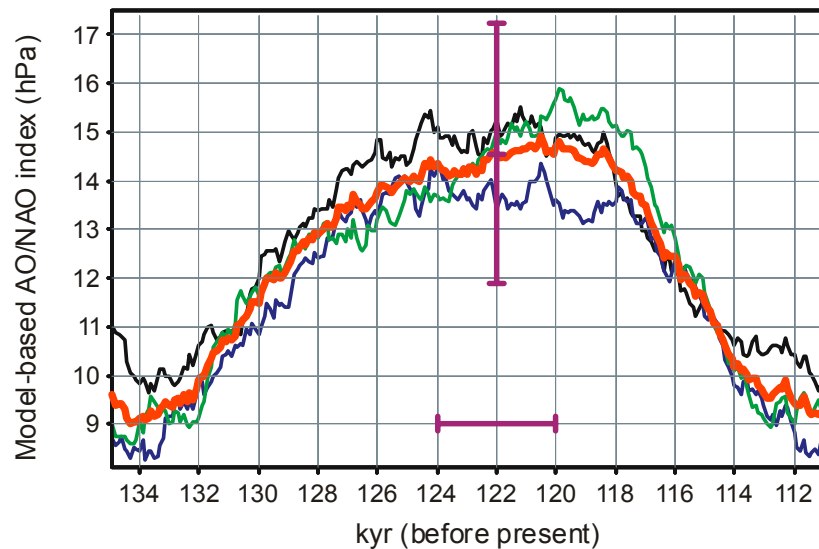
Figure S11 (Supplementary Figure 11) Modelled AO/NAO index for the last interglacial. Modelled AO/NAO index (December, January, February; DJF), defined as the sea level pressure difference between a southerly high pressure region and a northerly low pressure region (see Supplementary Fig. S7) for the last interglacial. A centred 41 year running mean for each of the three individual ensemble members has been applied (thin lines). The thick red line displays the ensemble mean. The vertical purple bar indicates the average and the mean standard deviation of the three experiments, taken from 41 years (DJF) marked by the horizontal purple bar (see Methods). The average (mean standard deviation) for 41 winters centred at 122 kyr, 3 kyr, and the pre-industrial period are 14.6 (5.3) hPa, 12.6 (4.8) hPa, and 11.7 (4.4) hPa, respectively (see also Fig. 3f).

SUPPLEMENTARY INFORMATION, Felis

Coral diagenesis

The two fossil corals are exceptionally well preserved given their ages. Due to the arid environment, the influence of meteoric water is minimized compared to fossil corals from the wet tropics. Diagenetic alterations, visible as areas of relatively high density in the X-radiograph positive prints due to secondary fillings of the skeletal pores and a resulting destruction of the annual banding pattern, can be identified along the outer margin of the corals as well as in restricted areas within the colonies (Fig. 1b, c). The X-radiograph positive prints were used as a guide to identify areas that appear to be unaffected by these alterations. These areas were investigated in more detail using X-ray powder diffraction and petrographic thin sections. X-ray diffraction analyses, performed at the Department of Mineralogy of the Faculty of Geosciences at Bremen University (Germany), indicate an aragonite content of the calcium carbonate of 99% and 98% for coral AQB-10-B (2.9 kyr) and coral AQB-3-A (122 kyr), respectively. Thin sections, prepared at the Department of Historical Geology/Palaeontology of the Faculty of Geosciences at Bremen University, reveal that skeletal elements are occasionally coated with a thin layer (<20 μm thick) of secondary aragonite, with no obvious difference between the two fossil corals. In addition, traces of calcite spar and patches of gypsum were present in coral AQB-3-A. Due to its concentration in specific regions the gypsum was also identifiable in the X-radiographs. Apart from the minor cementation, the skeletal material itself showed no signs of alteration.

The selected areas were used for further analyses (stable isotopes, Sr/Ca, radiocarbon and U-series dating). The time series of both coral $\delta^{18}O$ and $\delta^{13}C$ (not shown) show clear annual cycles, suggesting that the two fossil corals were not subject

to strong diagenetic alterations along the sampled profile with respect to stable isotopes. In contrast, coral Sr/Ca ratios of colony AQB-3-A show annual cycles only in a restricted section along the sampling profile. Only this part of the Sr/Ca time series was interpreted. That diagenesis has a greater impact on coral Sr/Ca than on $\delta^{18}O$ is in agreement with studies on fossil corals from other locations[15-17]. Comparing the section of coral AQB-3-A where Sr/Ca shows annual cycles with the section where these cycles are not observed reveals similar mean coral $\delta^{18}O$ values (-2.99‰ versus -2.91‰) and coral $\delta^{18}O$ derived temperature seasonality (8.4 °C versus 8.3 °C). X-radiographs reveal no obvious difference in the seasonal density banding pattern between these sections; and thin sections do not show evidence that diagenetic alteration progressed as a function of skeletal density. We therefore argue that the seasonal cycles of coral Sr/Ca and $\delta^{18}O$ interpreted from colony AQB-3-A are representative of the original climate conditions during the last interglacial. Thermal ionization mass spectrometry U-series dating indicates that especially coral AQB-3-A is diagenetically altered with respect to the U-Th system, and an appropriate correction of the U-series ages was applied[18]. That the U-Th isotopic system is more sensitive to diagenetic alterations than any petrographic or general geochemical parameter is in agreement with studies from other locations showing that even apparently pristine fossil corals can have a disturbed U-Th system[19,20].

In summary, we conclude that despite the facts that (1) minor amounts of secondary aragonite are observed in the two fossil corals and (2) subtle diagenetic processes in coral AQB-3-A affected the U-Th system and in some parts the Sr/Ca ratios, it is still possible to extract paleoclimatic information from these corals based on seasonal resolution time series of stable isotopes and Sr/Ca. This is in agreement with studies on fossil corals from other locations[15-17].

SUPPLEMENTARY INFORMATION, Felis

Sr/Ca analyses

For Sr/Ca analyses a 250-300 μg split from the sample powder that was used for $\delta^{18}O$ analyses was digested in 2% HNO_3. Y was added as internal standard to the sample solution. Measurements were carried out on a Finnigan Element2 High-Resolution Inductively Coupled Plasma Mass Spectrometer at the Faculty of Geosciences at Bremen University (Germany). Elemental concentrations in the sample solution were determined on the isotopes ^{48}Ca and ^{87}Sr. The calibrations were based on a blank and four standards prepared from an appropriately diluted stock solution. To correct for the instrumental drift during a sequence run, a laboratory internal coral standard of defined Sr/Ca ratio was measured after every third sample, and a drift correction was applied offline to all data. The internal precisions of the elemental concentrations were better than 0.2% relative standard error. The Sr/Ca ratios of 40 coral samples were determined in duplicate on different days; the average difference between two replicates was 0.02 mmol/mol.

SUPPLEMENTARY INFORMATION, Felis

1.   Nadeau, M.-J. *et al.* Sample throughput and data quality at the Leibniz-Labor AMS facility. *Radiocarbon* **40,** 239-245 (1998).

2.   Felis, T. *et al.* A coral oxygen isotope record from the northern Red Sea documenting NAO, ENSO, and North Pacific teleconnections on Middle East climate variability since the year 1750. *Paleoceanography* **15,** 679-694 (2000).

3.   Heiss, G. A. Coral reefs in the Red Sea: growth, production, and stable isotopes. *GEOMAR Report* **32,** 1-141 (1994).

4.   Stuiver, M., Pearson, G. W. & Braziunas, T. F. Radiocarbon age calibration of marine samples back to 9000 cal yr BP. *Radiocarbon* **28,** 980-1021 (1986).

5.   Stuiver, M. *et al.* INTCAL98 radiocarbon age calibration 0-24,000 BP. *Radiocarbon* **40,** 1041-1083 (1998).

6.   Rimbu, N., Lohmann, G., Felis, T. & Pätzold, J. Arctic Oscillation signature in a Red Sea coral. *Geophys. Res. Lett.* **28,** 2959-2962 (2001).

7.   Kalnay, E. *et al.* The NCEP/NCAR 40-year reanalysis project. *Bull. Amer. Meteor. Soc.* **77,** 437-472 (1996).

8.   Rayner, N. A., Horton, E. B., Parker, D. E., Folland, C. K. & Hackett, R. B. *Version 2.2 of the Global sea-Ice and Sea Surface Temperature data set, 1903-1994* (Hadley Centre, U. K. Meteorological Office, Bracknell, England, 1996).

9.   Berger, A. L. Long-term variations of daily insolation and Quaternary climatic changes. *J. Atmos. Sci.* **35,** 2362-2367 (1978).

10.   Thompson, D. W. J. & Wallace, J. M. Regional climate impacts of the Northern Hemisphere Annular Mode. *Science* **293,** 85-89 (2001).

11.   Boden, T. A., Kaiser, D. P., Sepanski, R. J. & Stoss, F. W. Trends '93: A compendium of data on global change. *ORNL/CDIAC-65*, Carbon Dioxide Information Analysis Center, Oak Ridge National Laboratory, Oak Ridge, Tenn., USA (1994).

12.   Machida, T., Nakazawa, T., Fujii, Y., Aoki, S. & Watanabe, O. Increase in the atmospheric nitrous oxide concentration during the last 250 years. *Geophys. Res. Lett.* **22,** 2921-2924 (1995).

13.   Etheridge, D. M. *et al.* Natural and anthropogenic changes in atmospheric CO_2 over the last 1000 years from air in Antarctic ice and firn. *J. Geophys. Res.* **101,** 4115-4128 (1996).

14.   Etheridge, D. M., Steele, L. P., Francey, R. J. & Langenfels, R. L. Atmospheric methane between 1000 A.D. and present: Evidence of anthopogenic emissions and climate variability. *J. Geophys. Res.* **103,** 15979-15993 (1998).

15.   Hughen, K. A., Schrag, D. P., Jacobsen, S. B. & Hantoro, W. El Niño during the last interglacial period recorded by a fossil coral from Indonesia. *Geophys. Res. Lett.* **26,** 3129-3132 (1999).

16.   Tudhope, A. W. *et al.* Variability in the El Niño-Southern Oscillation through a glacial-interglacial cycle. *Science* **291,** 1511-1517 (2001).

17.   McGregor, H. V. & Gagan, M. K. Diagenesis and geochemistry of *Porites* corals from Papua New Guinea: Implications for paleoclimate reconstruction. *Geochim. Cosmochim. Acta* **67,** 2147-2156 (2003).

18.   Scholz, D., Mangini, A. & Felis, T. U-series dating of diagenetically altered fossil reef corals. *Earth Planet. Sci. Lett.* **218,** 163-178 (2004).

19.   Hamelin, B., Bard, E., Zindler, A. & Fairbanks, R. G. $^{234}U/^{238}U$ mass spectrometry of corals: How accurate is the U-Th age of the last interglacial period? *Earth Planet. Sci. Lett.* **106,** 169-180 (1991).

20.   Zhu, Z. R. *et al.* High-precision U-series dating of Last Interglacial events by mass spectrometry: Houtman Abrolhos Islands, western Australia. *Earth Planet. Sci. Lett.* **118,** 281-293 (1993).